Precambrian Research 405 (2024) 107350

Contents lists available at ScienceDirect

Precambrian Research

journal homepage: www.elsevier.com/locate/precamres

Non-zero I/(Ca + Mg) recorded in Archean and Paleoproterozoic shallow marine Ca-carbonate sediments

Hao Fang [a,b,c], Philip Fralick [d], Brittany Ramsay [e], Dongjie Tang [a,b,f,*], Robert Riding [g]

[a] Frontiers Science Center for Deep-time Digital Earth, China University of Geosciences (Beijing), Beijing 100083, China
[b] State Key Laboratory of Biogeology and Environmental Geology, China University of Geosciences (Beijing), Beijing 100083, China
[c] Institute of Sedimentary Geology, Chengdu University of Technology, Chengdu 610059, China
[d] Department of Geology, Lakehead University, Thunder Bay, ON P7B 5E1, Canada
[e] Department of Geological Sciences and Geological Engineering, Queens University, Kingston, ON K7L 3N6, Canada
[f] Institute of Earth Sciences, China University of Geosciences (Beijing), Beijing 100083, China
[g] Department of Earth and Planetary Sciences, University of Tennessee, Knoxville, TN 37996, USA

ARTICLE INFO

Keywords:
Archean
Carbonate
Iodate
Marine
Oxygenation
Paleoproterozoic
Sedimentary geochemistry

ABSTRACT

Marine oxygenation during the Archean and Paleoproterozoic is poorly constrained. Iodine in carbonate is a possible oxygen indicator. We obtained molar ratios of iodine to calcium-magnesium [I/(Ca + Mg)] for 2.93–2.31 Ga from shallow marine Ca-carbonate (limestone, dolostone) platform sediments at several locations in the southern Superior Province in Canada and the USA. Maximum I/(Ca + Mg) ratios obtained are 0.13, 0.26, 0.05 and 0.22 μmol/mol, for 2.93, 2.86, 2.80 and 2.31 Ga samples, respectively. These non-zero carbonate I/(Ca + Mg) ratios indicate localized oxygen in Archean and Paleoproterozoic shallow marine environments. These data support an early origin for biological oxygen-production and, specifically, the idea that mid-late Archean oxygenation was sufficient to facilitate Ca-carbonate precipitation in shallow marine 'oxygen oases' adjacent to anoxic iron-rich seas

1. Introduction

Oxygenation transformed Earth's life and environments (Holland, 2006), but its inception and early history remain unclear (Catling and Zahnle, 2020; Kadoya et al., 2020; Ostrander et al., 2021). Stepwise oxygenation over the past 3.5 Ga, with marked increases ~ 2.4 Ga (Great Oxygenation Event, GOE) and ~ 0.8 Ga (Neoproterozoic Oxygenation Event, NOE) (Lyons et al., 2014; Krause et al., 2018; Poulton et al., 2021), has been attributed to long-term changes in the sources and sinks for oxygen mediated by biogeochemical cycling of carbon, oxygen, and phosphorus (Mills et al., 2014; Alcott et al., 2019; Bayon et al., 2022). Rates of oxygen production and consumption have been related to the effects of increasing Earth rotation rate on biotic evolution, nutrient and light availability (Klatt et al., 2021). Geochemical indicators, including decline in mass-independent sulfur isotope fractionation (Farquhar et al., 2000), suggest significant rise in atmospheric oxygen ~ 2.4 Ga (GOE) (Bekker et al., 2004; Holland, 2006). Prior to this, during the Archean, the rock record is more limited and often less well preserved. Available evidence, based on a wide variety of biological, geochemical and sedimentary indicators (summarized, e.g., by Buick, 2008; Fralick and Riding, 2015; Catling and Kasting, 2017; Catling and Zahnle, 2020; Ostrander et al., 2021) indicate that Archean oxygenation was often limited in time, extent and intensity (Olson et al., 2013; Eickmann et al., 2018; Ossa et al., 2019). Geochemical indicators suggest that mid-late Archean marine oxygenation (Anbar et al., 2007; Buick, 2008; Ostrander et al., 2020) included areas of shallow-water Ca-carbonate (limestone, dolostone) precipitation adjacent to otherwise Fe-rich marine basins (Klein and Beukes, 1989; Sumner, 1997; Kendall et al., 2010; Eickmann et al., 2018; Wang et al., 2020). Localized photosynthetic oxygenation may have removed sufficient Fe^{2+} from shallow water to promote the precipitation of aragonite and other Ca-carbonate minerals, rather than Fe-carbonate (siderite), as at Steep Rock Lake, Ontario, where at least ~ 10 μM oxygen concentration in seawater would have been required to accomplish this (Riding et al., 2014). These observations support the existence of marginal marine 'oxygen oases' (Fischer, 1965; Hayes, 1983; Kasting, 1992) that were significant in promoting the accumulation of carbonate platforms during the mid-Archean (~3.5–2.8 Ga) (Riding et al., 2014, 2022).

* Corresponding author at: Frontiers Science Center for Deep-time Digital Earth, China University of Geosciences (Beijing), Beijing 100083, China.
E-mail address: dongjtang@126.com (D. Tang).

https://doi.org/10.1016/j.precamres.2024.107350
Received 16 December 2023; Received in revised form 27 February 2024; Accepted 4 March 2024
Available online 13 March 2024

Numerous proxies have been used to recognize and track Earth's oxygenation during the Precambrian and Phanerozoic. These include Ce anomaly, I/Ca (or I/(Ca + Mg)), iron, chromium and molybdenum isotopes, and concentrations of manganese, selenium, sulfur, uranium, etc. (Tostevin and Mills, 2020; Kendall, 2021; Liu et al., 2021). Some of these approaches have been calibrated with oxygen, e.g., uranium (Rolison et al., 2017) and Fe (Poulton and Canfield, 2005), but others have not and consequently do not indicate absolute values of oxygen in air or water in the past (Tostevin and Mills, 2020). I/Ca or I/(Ca + Mg) has been used to indicate marine oxygenation over geological time (Liss, 1973; Lu et al., 2010, 2018; Hardisty et al., 2014, 2017; Shang et al., 2019). Analyses by Hardisty et al. (2014) showed no iodate in carbonate samples prior to ~ 2.3 Ga.

Here we report non-zero carbonate I/(Ca + Mg) measurements in Archean and early Proterozoic marine Ca-carbonate sediments. These results shed new light on shallow seawater redox conditions prior to the GOE and support inference of oxygen oases in otherwise oxygen-depleted oceans.

2. Geological setting and samples

We analyzed mid-Archean and early Paleoproterozoic samples for I/(Ca + Mg) from calcite and dolomite sediments deposited in the photic zones of thick carbonate platforms in the western Canadian Shield of central North America. These include Red Lake carbonate platform (2.93 Ga, Corfu and Wallace, 1986), Woman Lake carbonate platform (2.870 Ga, Rogers, 2002; 2.857 ± 0.005 Ga, Ramsay, 2020), Steep Rock Lake carbonate platform (Mosher Carbonate, 2.8 Ga; Fralick et al., 2008), and the Huronian Gordon Lake Formation (2.31 Ga, Rasmussen et al., 2013; Fig. 1). These deposits represent most of the thick carbonate accumulations preserved in the Superior Province, the largest Archean craton in existence.

Despite wide differences in the ages of our samples, they are all from marine carbonate platforms. These samples were deposited in environments ranging from nearshore (e.g., Woman Lake) and locally evaporitic (e.g., Gordon Lake), through platform interior (Red Lake) to platform margin (Steep Rock Lake, Red Lake) settings. Precise estimation of maximum water depths is difficult, but widespread presence of stromatolites, and local occurrences of grainstones, sheet-cracks and ripple marks, are all consistent with shallow-water deposition in these environments, most likely within the photic zone. Thin but laterally extensive crystal crusts of radial fans (thought to have been originally aragonite) (Steep Rock, Fralick and Riding, 2015), and herringbone calcite (Red Lake, McIntyre and Fralick, 2017), suggest incursions of anoxic offshore water onto the platforms. The presence of thick 'Giant Dome' accumulations at Steep Rock, and sporadic large dome development at Red Lake, are consistent with vigorous precipitation localized near platform margin chemoclines (Riding et al., 2022). These features are all consistent with sustained carbonate platform development that locally maintained extensive shallow-water conditions for substantial periods of time, estimated to be of the order of 5 Myr at Steep Rock (Riding et al., 2014). Together, the Red Lake (~200 m), Woman Lake (~110 m) and Steep Rock (~500 m) deposits represent the earliest successive development of relatively thick carbonate platforms currently known from the Archean, and are all associated with coeval deposition of iron formation in adjacent offshore anoxic ferruginous basins (Huston, 1956; Ramsay, 2020; Afroz et al., 2023). The 2.31 Ga Gordon Lake Formation and Kona Dolomite are post-glacial deposits that include shallow-water carbonates and local evaporites.

2.1. Red Lake

The 2.93 Ga Red Lake carbonate platform is currently Earth's oldest known thick (~200 m, McIntyre and Fralick, 2017) accumulation of Ca-

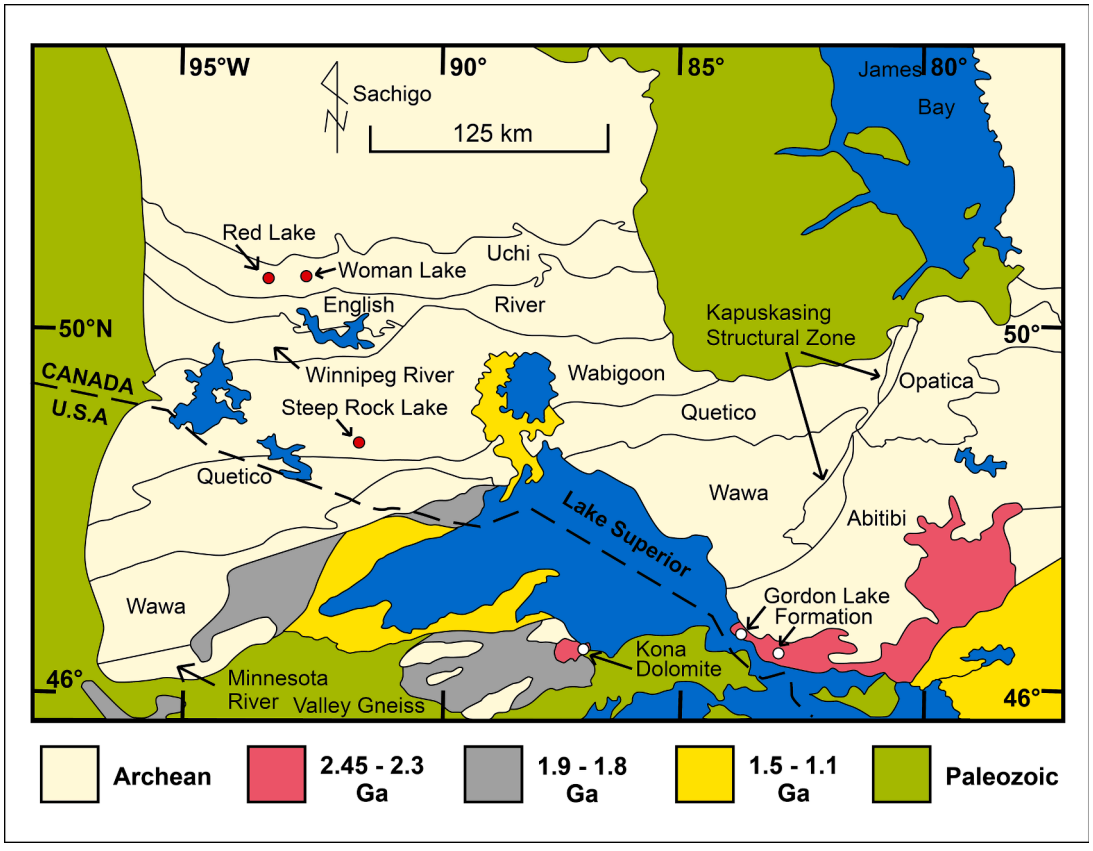

Fig. 1. Locations sampled in the Archean (red spots) and Paleoproterozoic (white spots) in the southern Superior Province of Canada and the USA, central North America.

carbonate sediment. It overlies an extensive succession of plume-generated mafic and ultramafic volcanic flows (Sanborn-Barrie et al., 2001), and consists of mainly dolomitic shallow water facies (Hofmann et al., 1985). The predominant components include laterally linked and unlinked domal stromatolites, stratiform stromatolites, thin layers of crystal fans, parallel laminated carbonate with or without fenestrae, and grainstones with sporadic sheet cracks and herringbone cement; calcite pseudomorphs of aragonite crystal fan mounds developed further offshore (Hofmann et al., 1985; McIntyre and Fralick, 2017). Deposits interpreted to represent the marginal slope transition to deeper water oxide iron formation, chert and carbonaceous slate, include chemocline-related interlaminated calcite and magnetite (Riding et al., 2022), and slumps of carbonate debris with matrices of magnetite and/or carbonaceous slate (Afroz et al., 2023). Dolomite samples are: domal stromatolites (RL-41, RL-46, RL-50, RL-51, RL-64B), crystal fan layers (RL-45, RL-48, RL-52, RL-63), laminated carbonate (RL2-49a, 98 W-3.5), sheet crack cement (RL2-16, RL2-42), dolomitized herringbone calcite (RL2-35), wavy laminite (RL2-40). Calcite samples are: crystal fan mounds (RL-69, RL-76, RL-78), carbonate interlaminated with magnetite (RL2-11, RL2-10C), slumped carbonate (RL2-70, RL2-72). In addition, HA-labeled samples are from a succession that includes crystal fan mounds and parallel laminated calcite near the break-in-slope to deeper water (Afroz et al., 2023) (Table S1).

2.2. Woman Lake

The 110 m thick, 2.86 Ga Woman Lake carbonate platform (Ramsay et al., 2020; Ramsay, 2020) directly overlies rhyolitic tuff which forms the uppermost unit of a thick mafic volcanic edifice (Thurston, 1980). Correlative units to the north, at Narrow Lake and Shabu Lake, include hummocky cross-stratified grainstones and carbonates and iron hydroxide precipitates that may have been deposited below storm wave base. At Woman Lake the carbonates sampled are shallow water nearshore limestones (Ramsay et al., 2020; Ramsay, 2020). The basal carbonates are crinkly layered stratiform stromatolites interbedded with thin grainstones. These transition upward into laterally-linked low domes, then larger domes and bioherms with walled pseudo-columnar stromatolites, followed by cross-stratified grainstones and more pseudo-columnar stromatolites. These in turn are overlain by carbonates including fenestral microbialite, zig-zag lamination, thrombolite-like fabrics, stromatactis-bearing low domal stromatolites, and narrow isolated columnar stromatolites, followed by a cyclic succession of low domal stromatolites alternating with microbial carbonate and carbonate grainstone (Hofmann et al., 1985; Ramsay, 2020).

All samples analyzed from Woman Lake are primarily calcite without significant recrystallization or obvious post-depositional alteration (Ramsay et al., 2020; Ramsay, 2020). They include: domal stromatolites (WM-65, WM-129Q, A-1, A-14, A-18A, A-23, A-52, A-56, X-3Q), stratiform stromatolites (WM-58x, WM-115), fenestral stromatolites (X-16Q, X-10BT), fenestrate microbialite (A-2, A-9, A-28, X-14Y, X-24X, WM-113, WM-114X, WM-109, WM-112), fenestral carbonate (X-10BQ), banded carbonate (WM-107y), zig-zag lamination (X-12), and grainstone (A-39, WM-64, WM-71A, WM-74, X-6S) (Table S1).

2.3. Mosher Carbonate, Steep Rock Lake

The ~ 500 m thick, 2.8 Ga Mosher Carbonate was deposited on an oceanic volcanic plateau (Fralick et al., 2008) formed by plume activity (Hollings et al., 1999). As such it represents an isolated, rimmed carbonate platform. The shallow water rim includes a thick succession of overlapping meter-scale 'Giant Domes', each internally mainly consisting of alternating layers of formerly aragonitic crystal fans and cuspate fenestral microbialite (Fralick and Riding, 2015). The inner platform contains stratiform and small domal calcite stromatolites, locally forming small bioherms, with scarce layers of crystal fan crust and pseudo-columnar and branching dolomite stromatolites (Fralick and Riding, 2015). Ultimately, marine flooding of the carbonate platform deposited overlying manganiferous iron formation, grading distally (basinward) to iron formation containing lesser amounts of Mn (Huston, 1956). These sediments, together with platform margin crystal fan (formally aragonite) crusts that contain negative Ce anomalies, and the calcite stromatolites of the platform interior that preserve thin zones of ferroan dolomite alteration, are consistent with marine oxygenation, presumably by cyanobacteria, that permitted precipitation of Ca-carbonate in an 'oxygen oasis', delimited basinward by a chemocline at which manganiferous iron formation was deposited (Riding et al., 2014, 2022). Progressive onshore decline in dissolved Fe at the chemocline allowed the successive precipitation of first aragonite and then calcite within the 'Giant Domes' that form the platform margin (Fralick and Riding, 2015; Riding et al., 2022). Lithotypes sampled include: crystal fan (SR-16A, SR-18A, SR-18E, SR-22A, 8–26), microbialite associated with crystal fan (SR-16B, SR-18C, SR-18D, SR-22B), cement associated with crystal fan (SR-18B), stratiform and small domical stromatolites (8–20, 8–21, 8–24, 8–33, SR-5A), cement associated with small domical stromatolites (SR-5B), parallel laminated carbonate (SR-2A, SR-2B, SR-9, SR-7), grainstone (8–28, 8–31), and dolomite pseudo-columnar stromatolites (8-43B, 8-44B) (Table S1).

2.4. Kona dolomite and Gordon Lake formation

The 2.31 Ga Gordon Lake Formation (Canada) and Kona Dolomite (USA) represent post-glacial sediments that extend ~ 400 km west-east from north of Lake Michigan to north of Lake Huron (Chandler, 1988), dominated by dolomite in the west and siliciclastics in the east. Depositional environments range from supratidal gypsiferous-dolomitic flats with halite-bearing salinas, through micritic stromatolitic intertidal intervals to shallow offshore carbonates with hummocky cross-stratified and ripple laminated grainstones and 3 m high stromatolitic bioherms (Taylor, 1972; Wood, 1973; Robertson, 1973; Frarey, 1977; Hofmann et al., 1980; Wohlabaugh, 1980; Wright and Rust, 1985; Bennett, 2006; Ramsay, 2017; Ramsay and Fralick, 2017). This assemblage was deposited during the GOE, near the beginning of the Lomagundi positive $\delta^{13}C$ excursion (Bachan and Kump, 2015; Ramsay, 2017). At that time, rising atmospheric oxygen levels were resulting in increased delivery of oxidized iron and other metals to the sea (Konhauser et al., 2011). Sampled lithologies include: large stromatolitic bioherms (BK-5X) and hummocky cross-stratified grainstone (BK-1X) deposited offshore; rippled grainstone (BQ-1Y), parallel laminated micrite (BD-2X, BQ-2Y) and small domal stromatolites (BQ-3X, BQ-6X) representing shore-proximal lagoon and tidal flat deposits; and sabkha (evaporative tidal flat) dolomite layers with pseudomorphs of gypsum crystals (BH-6X, BP-1X, BH-3X) within flood deposited siliciclastics (Ramsay, 2017) (Table S1). Samples from this succession that were analyzed for iodine by Hardisty et al. (2014) were obtained from upper tidal flat fenestral microbialite, resedimented carbonate within siliciclastic pebble to cobble conglomerate, and an area with small stromatolites.

3. Methodology

All samples were collected from surface outcrops, except for samples designated A, which are from a 6 m interval drilled in the Woman Lake succession. Glaciers retreated from the study areas approximately 9,000 years ago, leaving surfaces eroded down to fresh rock, which has since undergone only very minor chemical weathering in the cold climate. Any weathered rinds were removed from samples prior to processing.

For iodine analysis, samples of fresh, unaltered carbonate rock were crushed with a tungsten-carbide mallet and powdered in an agate mill. A ~ 4 mg dry powder sub-sample was rinsed three times in Milli-Q water and digested using 4 mL 3 % nitric acid in 15 mL centrifuge tubes. This partial dissolution technique was used to target carbonate and exclude siliciclastic and phosphatic material. The influence of detrital components was further assessed by comparing the Al and iodate

concentrations. Following 0.5-hour digestion, the supernatant was collected and 1 mL was used for iodine analysis. 3 % tertiary amine solution was added to stabilize the iodine (Hardisty et al., 2017; Lu et al., 2010). Antimony (Sb) was spiked into the solution (0.3 ppm) as an internal standard to monitor and correct the sensitivity of the instrument. The supernatant was ultimately diluted to ~ 1:6000 and Ca concentration was maintained at ~ 50 ppm. Iodine content was then measured using a Multicollector-Inductively Coupled Plasma-Mass Spectrometer (MC-ICP-MS) (Neptune Plus, Thermo Fisher Scientific, Germany) at the National Research Center of Geoanalysis, Beijing. The sensitivity of iodine was tuned to ~ 1500 kcps for a 1 ppb standard in the MC-ICP-MS. Replicates of individual samples were analyzed from re-digestion of bulk-rock samples. The detection limit of iodine, determined using duplicates of blank samples, was 0.02 ppm (Table S2). The analytical uncertainty and accuracy of ^{127}I, monitored by certified reference material JDo-1, were 5.8 % and 99.8 %, respectively (Table S3). The standard deviation of I/(Ca + Mg) of reference material JDo-1 is 0.03 μmol/mol. For Ca and Mg content, 0.2 mL supernatant was diluted to 1:51000 with 3 % nitric acid. Ca and Mg concentrations were measured using a PerkinElmer NexION 300Q ICP-MS at the National Research Center for Geoanalysis, Beijing, following the method described by Liu et al. (2020). Certified reference material JDo-1 (dolostone) was repeatedly measured every 10 samples. The analytical uncertainties monitored by JDo-1 were 4.9 % for Mg and 3.7 % for Ca (Table S3).

4. Results

4.1. Results of our I/(Ca + Mg) data

Our analytical results of I/(Ca + Mg) are tabulated by location, geological age, and lithology (Table S1). The wide range of primary rock fabrics represented include: rippled grainstone (BQ-1Y) and parallel laminated micrite (BQ-2Y) at Gordon Lake; grainstones (8–31) at Steep Rock Lake; domal stromatolites (WM-65, A-18A, A-52), fenestral stromatolites (X-16Q, X-10BT), fenestral microbialite (A-9, X-14Y, WM-114X, WM-109), fenestral carbonate (X-10BQ), and grainstone (A-39, WM-71A) at Woman Lake (Fig. 2); crystal fan layers (RL-52), carbonate interlaminated with magnetite (RL2-11), and slumped carbonate (RL2-72) at Red Lake (Table S1). Initially, all samples were analyzed. Those showing a non-zero result (20 out of a total of 104 samples), were then reanalyzed four times. For each sample, we report the maximum I/(Ca + Mg) ratio among the five analyses, since diagenetic effects are only known to lower original values (e.g., Hardisty et al., 2014). The maximum I/(Ca + Mg) data (Table 1 and Table S1) show a wide range of non-zero, albeit low, values (Fig. 3). For each location, the maximum non-zero values were averaged according to the total number of samples that were above the detection limit. This could underestimate the average I/(Ca + Mg) ratio, but not the maximum value. For example, analyses of multiple Woman Lake samples show maximum I/(Ca + Mg) in the range 0.02–0.26 μmol/mol, with the average maximum value being 0.08 μmol/mol (Table 1).

5. Discussion

Previous studies of I/(Ca + Mg) in limestone have estimated levels of marine oxygenation for the past 3 billion years (e.g., Liss, 1973; Lu et al., 2010, 2018; Hardisty et al., 2014, 2017; Shang et al., 2019). Until now, so far as we are aware, only zero I/(Ca + Mg) ratios have been reported for Archean samples (Hardisty et al., 2014, 2017; Hodgskiss and Sperling, 2021, and references therein). Iodine is used as an oxygen proxy because oxidized iodate has been regarded as the only iodine species to be incorporated in carbonates under oxygenated conditions, whereas reduced iodide is not incorporated (Lu et al., 2010). Since iodate tends to be quantitatively reduced to iodide in oxygen-depleted conditions (Emerson et al., 1979), iodate in carbonate may be a proxy indicator of oxygen for shallow seawater where carbonate precipitated (Lu et al., 2010, 2018; Hardisty et al., 2014, 2017; Shang et al., 2019). However, scaling up to global ocean and atmospheric O_2 using the iodate proxy is not appropriate because iodate transport and its slow reduction in deep water results in disequilibrium between iodine species in the present-day ocean (Hardisty et al., 2021). Nonetheless, semi-quantitative oxygen estimates based on iodate in carbonate values have been made for the Phanerozoic and Proterozoic (e.g., Hardisty et al., 2014; Lu et al., 2016; Shang et al., 2019).

Oxygen produced by cyanobacterial photosynthesis in shallow seawater is widely thought to have been the initial significant source of oxygen in the Precambrian ocean (Cloud, 1968; Holland, 2006; Catling and Kasting, 2017; Catling and Zahnle, 2020) and atmosphere (Crowe et al., 2013; Planavsky et al., 2014). However, this may only have amounted to about 1–10 μM in the Precambrian ocean (Kasting, 1991; Olson et al., 2013; Reinhard et al., 2013, 2016). Atmospheric oxygen levels could have remained low (e.g., < 2.5% PAL), while oxygen production in shallow seawater produced higher dissolved oxygen in water (Reinhard et al., 2016). Moreover, due to the rapid consumption of

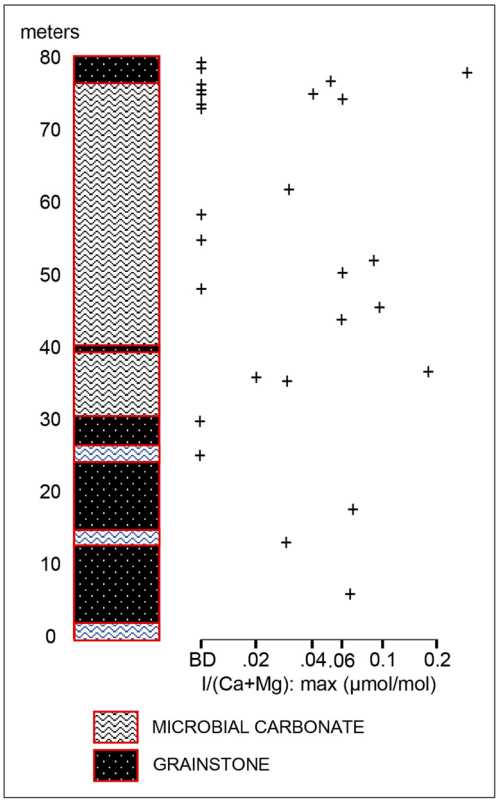

Fig. 2. A diagrammatic representation of the Woman Lake Carbonate Platform stratigraphic column with corresponding I/(Ca + Mg). Microbial carbonate and grainstone compose most of the studied interval.

Table 1
Summary of I/(Ca + Mg) data measured in carbonates in this study.

Location	Age (Ga)	Non-zero data/ total number of analyses	Range of maximum I/(Ca + Mg) (μmol/mol)	Average of maximum I/(Ca + Mg) (μmol/mol)
Gordon Lake	2.31	3/10	0.04–0.22	0.12
Steep Rock Lake	2.8	1/24	0.05–0.05	0.05
Woman Lake	2.86	15/31	0.02–0.26	0.08
Red Lake	2.93	4/29	0.04–0.13	0.08

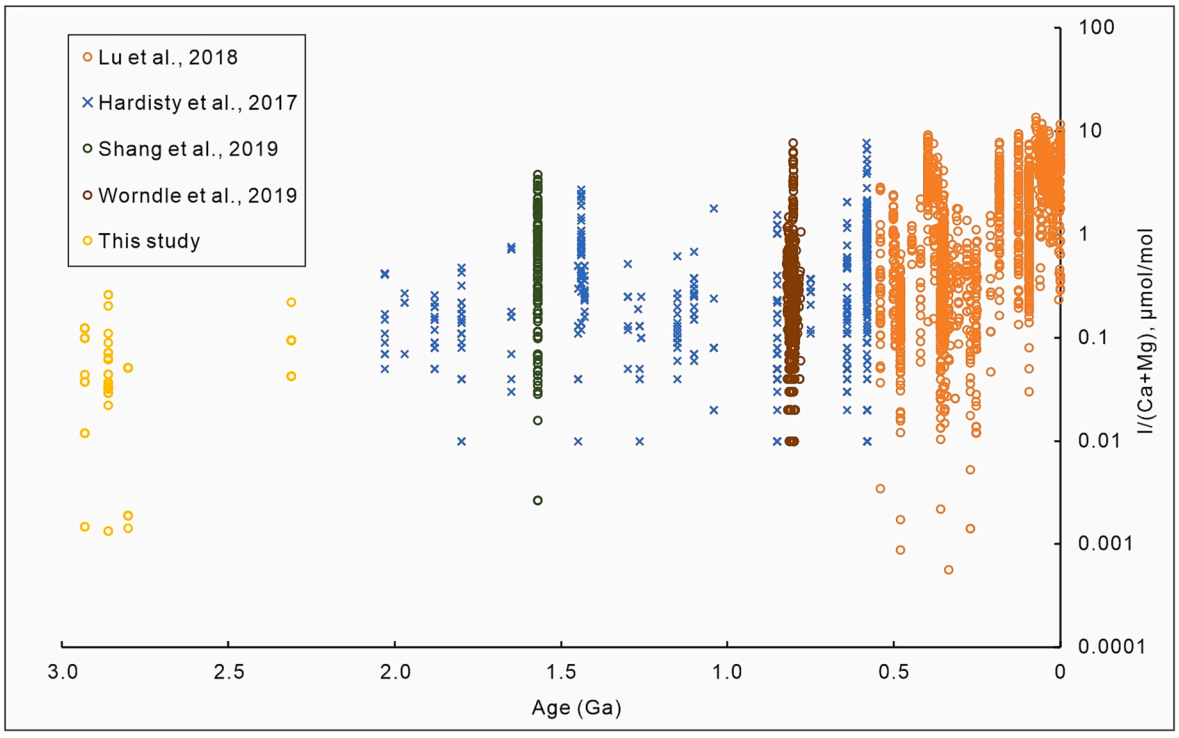

Fig. 3. Compilation of I/(Ca + Mg) reported in Archean and Proterozoic carbonates.

reductants in relatively shallow seawater prior to the GOE (Canfield, 2005; Holland, 2006), oxygen generally accumulated locally, as suggested by previous data (Riding et al., 2014). Thus, the disequilibrium presence of seawater oxygen generates variant patterns of redox proxies. For Archean carbonates, our study detected iodine in nearly half of the samples (15/31) from 2.86 Ga Women Lake together with a few non-zero values from the other 3 sections (Table 1). Based on previous studies and supported by present-day observations (e.g., Hardisty et al., 2014, 2017; Luther and Campbell, 1991; Rue et al., 1997), > 0.1 µmol/mol of I/(Ca + Mg) has been suggested as an indicator of water-column oxygen > 1–3 µM (Shang et al., 2019). Although our I/(Ca + Mg) data may not be able to quantitatively constrain either seawater or atmospheric oxygen concentrations, the occurrence of carbonate-bonded iodate is a clear indication that oxygen was available, at least locally, in seawater in the mid- to late-Archean. This is consistent with the appearance of cyanobacteria 3.6–3.3 Ga, long suspected from recognition of cyanobacteria-like structures (Awramik et al., 1983; Schopf, 2006), increasingly from phylogenetic studies (e.g., Boden et al., 2021), and also from a suite of additional chemical signatures for oxygen (e.g., Zhang and Shields, 2022).

Our analytical data show considerable within-sample and between-sample variation, with I/(Ca + Mg) measurements ranging from non-detectable to 0.26 µmol/mol. For example, analyses of multiple Woman Lake samples (Table 1 and Table S1) show maximum I/(Ca + Mg) in the range 0.02 to 0.26 µmol/mol, with the average maximum value being 0.07 µmol/mol. This variation is not due to analytical uncertainty (see Section 3) or to detrital components (Fig. 4 and Table S1). Within-sample variation may be attributed to diagenesis, as observed in other studies (e.g., Hardisty et al., 2017), and it appears that between-sample variation likely reflects differences in both primary components and diagenetic alteration. For example, non-zero I/(Ca + Mg) ratios at Woman Lake are from samples of domal stromatolites, fenestral stromatolites, fenestrate microbialite, fenestral carbonate, and grainstone. These can represent combinations of the effects of depositional environment and diagenetic alteration. Environmental differences could include variations in oxygen level in the water column and within

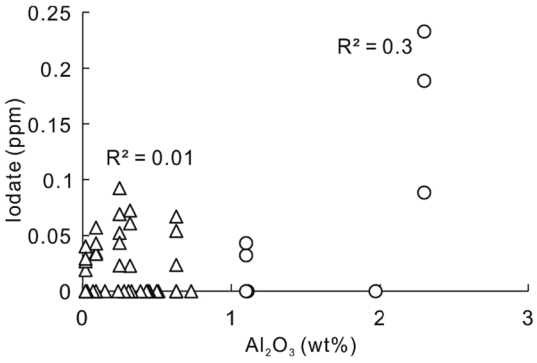

Fig. 4. Plot of iodate concentration against Al_2O_3 content. These data are listed in Table S1. The overall correlation coefficient (R^2) of ~ 0.3 shows that iodate is moderately correlated with detrital components. However, this correlation is due to two samples with high concentrations of Al_2O_3. The correlation coefficient between iodate and samples with Al_2O_3 < 1 wt% (triangles) is insignificant (R^2 = 0.01).

sediment pore-water. If iodate incorporation in carbonate occurred in both sediment pore-water and the water column, then measured I/(Ca + Mg) should reflect a combination of the dissolved O_2 levels in these adjacent sub-environments, and might therefore range from highly saturated O_2 to anoxic. In addition, the level of oxygen in the water column could vary laterally within the same general depositional environment. For example, platform interior oxygen levels might reflect seasonal variations in oxygen production. In contrast, near a chemocline at the platform margin, the presence of oxidizable components such as Fe^{2+} could rapidly deplete oxygen. Effects such as these could account for low, but non-zero, I/(Ca + Mg) ratios observed in 'Giant Dome' samples from the Steep Rock Lake platform margin, compared to platform interior samples from Woman Lake.

Carbonate iodate concentrations prior to the GOE were previously examined by Hardisty et al. (2014). Only zero I/(Ca + Mg) ratios were reported among the samples with ages > 2.5 Ga (Hardisty et al., 2014).

However, there are at least two major factors that might lead to misleading zero results. Since carbonate-bonded iodate is sensitive to diagenesis, the quality of preservation of the samples selected for I/(Ca + Mg) analysis is of vital importance. Due to the sample heterogeneity mentioned above, it is possible that iodate signals were obscured by dilution during analysis of bulk-rock powders. Previous investigations of Steep Rock, Woman Lake and Red Lake carbonate platforms using proxies other than iodine also provide reliable information regarding oxygenation. Although they are scarce, negative Ce anomalies occur in Red Lake carbonates (McIntyre and Fralick, 2017; Afroz et al., 2023), whereas the majority of magnetite iron formation samples, from units underlying and interlayered with these carbonates, have positive Ce anomalies (Afroz, 2019; Afroz et al., 2023). These latter studies also show that Mn concentrations increase towards the carbonate platform. Enrichment in redox sensitive elements, such as Cr, V, Mo and U, in Red Lake carbonates and magnetite may be explained by the siliciclastic components in these samples, further suggesting the presence of free oxygen in this system (Afroz et al., 2023). Significant negative Ce anomalies are abundant in limestone samples from Woman Lake, occurring in 89 of 152 samples analyzed (Ramsay, 2020). Similarly, samples of crystal fan and fenestral microbialite layers in Steep Rock hybrid 'Giant Domes' are dominated by negative Ce anomalies (Riding et al., 2014; Fralick and Riding, 2015). These have been cited as credible evidence for the presence of at least ephemeral free oxygen in Archean seawater (Zhang and Shields, 2022). Mo isotopes in these samples also indicate the presence of free oxygen (Thoby et al., 2019). The generation of oxygen in the surface waters of the Steep Rock carbonate platform would also account for the increase observed in MnO_2 in the associated offshore iron formation, from < 0.5 wt% in deeper water, to 19 wt% adjacent to the carbonates (Huston, 1956). Together, these proxies support the local presence of significant concentrations of free dissolved oxygen in these mid-Archean shallow-water carbonates.

I/(Ca + Mg) data reflect dissolved oxygen levels in the water from which the sediments were precipitated. These values can be converted to present-atmospheric level (PAL) if air–water equilibrium is assumed. However, atmospheric oxygen levels in the mid-Archean are expected to have been near zero ($\ll 10^{-5}$ PAL; Hardisty et al., 2014, Fig. 1). Consequently, it is likely that locally generated dissolved oxygen in these waters varied seasonally and was transient, due to the combined effects of local consumption and escape to the atmosphere. Similar considerations are appropriate for low oxygen concentration in seawater during the Proterozoic. For example, previously published iodate data suggest Proterozoic dissolved oxygen levels over 10 to ~70 μM (e.g., Hardisty et al., 2017; Shang et al., 2019; Wörndle et al., 2019). If these had been in equilibrium with the atmosphere, they would indicate maximum O_2 levels of ~4% PAL, higher than published estimates of atmospheric O_2 levels for much of the Proterozoic of ≤ 1% PAL (Hardisty et al., 2014, fig. 1; Lyons et al., 2014; Hardisty et al., 2017, fig. 6). However, this disparity only arises when global air–water equilibrium is assumed, rather than variation with local conditions and with the redox dynamics that occur in water and at the water–air interface. We therefore propose that only when atmospheric oxygenation was firmly established should air–water equilibrium be used to evaluate atmospheric oxygen level.

6. Conclusions

1. Non-zero values of I/(Ca + Mg) are measured in Archean marine carbonates for the first time.
2. These results are consistent with the interpretation that Archean carbonate platforms beside Fe-rich seas formed in 'oxygen oases', since in these conditions shallow marine oxygenation favored Ca-carbonate over Fe-carbonate precipitation.
3. O_2 buildup in Archean seawater was not only localized but transient. So long as oxidizable components, such as Fe^{2+}, were widely available to remove dissolved oxygen, atmospheric oxygenation (e.g., the GOE) could not progress. For this reason, the Archean values reported here are for water only and are not converted to partial pressure in % PAL. Consequently, until water-atmosphere O_2 equilibrium was firmly established (e.g., during the Phanerozoic) it could be inappropriate to use dissolved O_2 to infer atmospheric values.

CRediT authorship contribution statement

Hao Fang: Writing – review & editing, Writing – original draft, Methodology. **Philip Fralick:** Writing – review & editing, Investigation. **Brittany Ramsay:** Writing – review & editing, Investigation. **Dongjie Tang:** Writing – review & editing, Writing – original draft, Conceptualization. **Robert Riding:** Writing – review & editing, Writing – original draft, Conceptualization.

Declaration of competing interest

The authors declare that they have no known competing financial interests or personal relationships that could have appeared to influence the work reported in this paper.

Data availability

Data are available in the Supplementary Information.

Acknowledgements

This study was supported by the National Natural Science Foundation of China (nos. 41930320; 42372233), the Natural Science and Engineering Research Council of Canada, the Euro-pean Union's Horizon 2020 Research and Innovation Program (no. 716515), the "Deep-time Digital Earth" Science and Technology Leading Talents Team Funds for the Central Universities for the Frontiers Science Center for Deep-time Digital Earth, China University of Geosciences (Beijing) (Fundamental Research Funds for the Central Universities; no. 2652023001), and the Chinese "111" project (B20011). We thank Liyuan Liang for advice and discussion, and Limin Zhou for assistance during the experimental work. We greatly appreciate the comments of Eva Stüeken and an anonymous reviewer that improved the manuscript, and Frances Westall's expert editorial guidance.

Appendix A. Supplementary data

Supplementary data to this article can be found online at https://doi.org/10.1016/j.precamres.2024.107350.

References

Afroz, M., 2019. Sedimentology and geochemistry of the 2.93 Ga Basinal Facies of the Red Lake carbonate platform. Lakehead University, Thunder Bay, Canada, p. 157. MSc Thesis.
Afroz, M., Fralick, P.W., Lalonde, S.V., 2023. Sedimentology and geochemistry of basinal lithofacies in the Mesoarchean (2.93 Ga) Red Lake carbonate platform, Northwest Ontario, Canada. Precambr. Res. 388, 106996.
Alcott, L.J., Mills, B.J.W., Poulton, S.W., 2019. Stepwise Earth oxygenation is an inherent property of global biogeochemical cycling. Science 366, 1333–1337.
Anbar, A.D., Duan, Y., Lyons, T.W., Arnold, G.L., Kendall, B., Creaser, R.A., Kaufman, A. J., Gordon, G.W., Scott, C., Garvin, J., 2007. A whiff of oxygen before the great oxidation event? Science 317, 1903–1906.
Awramik, S.M., Schopf, J.W., Walter, M.R., 1983. Filamentous fossil bacteria from the Archean of Western Australia. Precambr. Res. 20, 357–374.
Bachan, A., Kump, L.R., 2015. The rise of oxygen and siderite oxidation during the Lomagundi Event. Proc. Natl. Acad. Sci. 112, 6562–6567.
Bayon, G., Bindeman, I.N., Trinquier, A., Retallack, G.J., Bekker, A., 2022. Long-term evolution of terrestrial weathering and its link to Earth's oxygenation. Earth Planet. Sci. Lett. 584, 117490.
Bekker, A., Holland, H.D., Wang, P.L., Rumble, D.I.I.I., Stein, H.J., Hannah, J.L., Coetzee, L.L., Beukes, N.J., 2004. Dating the rise of atmospheric oxygen. Nature 427, 117–120.
Bennett, G. (2006) The Huronian Supergroup between Sault Ste. Marie and Elliot Lake. Institute on Lake Superior Geology, 52nd Annual Meeting (Sault Ste. Marie, Ontario), Field Trip Guidebook, Pt. 4, 65 p.

Boden, J.S., Konhauser, K.O., Robbins, L.J., Sánchez-Baracaldo, P., 2021. Timing the evolution of antioxidant enzymes in cyanobacteria. Nat. Commun. 12, 4742.
Buick, R., 2008. When did oxygenic photosynthesis evolve? Philos. Trans. R. Soc., B 363, 2731–2743.
Canfield, D.E., 2005. The early history of atmospheric oxygen: homage to Robert M. Garrels. Annu. Rev. Earth Planet. Sci. 33, 1–36.
Catling, D.C., Kasting, J.F., 2017. Atmospheric evolution on inhabited and lifeless worlds. Cambridge University Press.
Catling, D.C., Zahnle, K.J., 2020. The Archean atmosphere. Sci. Adv. 6, eaax1420.
Chandler, F.W., 1988. Diagenesis of sabkha-related sulfate nodules in the Early Proterozoic Gordon Lake Formation, Ontario, Canada. Carbonates Evaporites 3, 75–94.
Cloud Jr, P.E., 1968. Atmospheric and hydrospheric evolution on the primitive earth. Science 160, 729–736.
Corfu, F., Wallace, H., 1986. U-Pb zircon ages for magmatism in the Red Lake greenstone belt, northwestern Ontario. Can. J. Earth Sci. 23, 27–42.
Crowe, S.A., Døssing, L.N., Beukes, N.J., Bau, M., Kruger, S.J., Frei, F., Canfield, D.E., 2013. Atmospheric oxygenation three billion years ago. Nature 501, 535–539.
Eickmann, B., Hofmann, A., Wille, M., Bui, T.H., Wing, B.A., Schoenberg, R., 2018. Isotopic evidence for oxygenated Mesoarchaean shallow oceans. Nat. Geosci. 11, 133–138.
Emerson, S., Cranston, R.E., Liss, P.S., 1979. Redox species in a reducing fjord: equilibrium and kinetic considerations. Deep Sea Res. Part A. Oceanogr. Res. Papers 26, 859–878.
Farquhar, J., Bao, H., Thiemens, M., 2000. Atmospheric influence of Earth's earliest sulfur cycle. Science 289, 756–758.
Fischer, A.G., 1965. NAS symposium on the evolution of the Earth's atmosphere: fossils, early life, and atmospheric history. Proc. Natl. Acad. Sci. USA 53 (6), 1205–1215.
Fralick, P., Hollings, P., King, D., 2008. Stratigraphy, geochemistry and depositional environments of Mesoarchean sedimentary units in western Superior Province: implications for generation of early crust. In: Condie, K.C., Pease, V. Eds., When did Plate Tectonics begin on Planet Earth? Geological Society of America Special Paper 440, 77–96.
Fralick, P., Riding, R., 2015. Steep rock Lake: sedimentology and geochemistry of an Archean carbonate platform. Earth Sci. Rev. 151, 132–175.
Frarey, M.J., 1977. Geology of the Huronian belt between Sault Ste. Marie and Blind River, Ontario. Geol. Survey Canada Memoir 383, 87 p.
Hardisty, D.S., Lu, Z., Planavsky, N.J., Bekker, A., Philippot, P., Zhou, X., Lyons, T.W., 2014. An iodine record of Paleoproterozoic surface ocean oxygenation. Geology 42, 619–622.
Hardisty, D.S., Lu, Z., Bekker, A., Diamond, C.W., Gill, B.C., Jiang, G., Kah, L.C., Knoll, A. H., Lloyd, S.J., Osburn, M.R., Lyons, T.W., 2017. Perspectives on Proterozoic surface ocean redox from iodine contents in ancient and recent carbonate. Earth Planet. Sci. Lett. 463, 159–170.
Hardisty, D.S., Horner, T.J., Evans, N., Moriyasu, R., Babbin, A.R., Wankel, S.D., Moffett, J.W., Nielsen, S.G., 2021. Limited iodate reduction in shipboard seawater incubations from the Eastern Tropical North Pacific oxygen deficient zone. Earth Planet. Sci. Lett. 554, 116676.
Hayes, J.M., 1983. Geochemical evidence bearing on the origin of aerobiosis, a speculative hypothesis. In: Schopf, J.W. (Ed.), Earth's Earliest Biosphere, Its Origin and Evolution. Princeton University Press, pp. 291–301.
Hodgskiss, M.S.W., Sperling, E.A., 2021. A prolonged, two-step oxygenation of Earth's early atmosphere: support from confidence intervals. Geology 50, 158–162.
Hofmann, H.J., Thurston, P. and Wallace, H. (1985) Archean stromatolites from Uchi greenstone belt, northwestern Ontario. In: Evolution of Archean Supracrustal Sequences. GAC St. Johns, Newfoundland, pp. 125–132.
Hofmann, H.J., Pearson, D.A.B., Wilson, B.H., 1980. Stromatolites and fenestral fabric in Early Proterozoic Huronian Supergroup, Ontario. Can. J. Earth Sci. 17, 1351–1357.
Holland, H.D., 2006. The oxygenation of the atmosphere and oceans. Philos. Trans. R. Soc., B: Biol. Sci. 361, 903–915.
Hollings, P., Wyman, D., Kerrich, R., 1999. Komatiite-basalt-rhyolite volcanic associations in northern Superior Province greenstone belts: significance of plume-arc interaction in the generation of the proto continental Superior Province. Lithos 46, 137–161.
Huston, W.J., 1956. The Steep Rock manganiferous footwall paint. Unpublished MSc. thesis, Queen's University, Kingston, Canada, 76 p.
Kadoya, S., Catling, D.C., Nicklas, R.W., Puchtel, I.S., Anbar, A.D., 2020. Mantle data imply a decline of oxidizable volcanic gases could have triggered the Great Oxidation. Nat. Commun. 11, 1–9.
Kasting, J.F., 1991. Box models for the evolution of atmospheric oxygen: an update. Palaeogeogr. Palaeoclimatol. Palaeoecol. 97, 125–131.
Kasting, J.F., 1992. Models relating to Proterozoic atmospheric and ocean chemistry. In: Schopf, J., Klein, C. (Eds.), The Proterozoic Biosphere: A Multidisciplinary Study: Cambridge. Cambridge University Press, UK, pp. 1185–1187.
Kendall, B., 2021. Recent advances in geochemical paleo-oxybarometers. Annu. Rev. Earth Planet. Sci. 49, 399–433.
Kendall, B., Reinhard, C.T., Lyons, T.W., Kaufman, A.J., Poulton, S.W., Anbar, A.D., 2010. Pervasive oxygenation along late Archaean Ocean margins. Nat. Geosci. 3, 647–652.
Klatt, J.M., Chennu, A., Arbic, B.K., Biddanda, B.A., Dick, G.J., 2021. Possible link between Earth's rotation rate and oxygenation. Nat. Geosci. 14, 564–570.
Klein, C., Beukes, N.J., 1989. Geochemistry and sedimentology of a facies transition from limestone to iron-formation deposition in the early Proterozoic Transvaal Supergroup, South Africa. Econ. Geol. 84, 1733–1774.
Konhauser, K.O., Lalonde, S.V., Planavsky, N.J., Pecoits, E., Lyons, T.W., Mojzsis, S.J., Rouxel, O.J., Barley, M.E., Rosière, C., Fralick, P.W., Kump, L.R., Bekker, A., 2011. Aerobic bacterial pyrite oxidation and acid rock drainage during the great oxidation event. Nature 478, 369–373.
Krause, A.J., Mills, B.J., Zhang, S., Planavsky, N.J., Lenton, T.M., Poulton, S.W., 2018. Stepwise oxygenation of the Paleozoic atmosphere. Nat. Commun. 9, 1–10.
Liss, P.S., 1973. Processes of gas exchange across an air-water interface. Deep-Sea Res. Oceanogr. Abstr. 20, 221–238.
Liu, X.M., Kah, L.C., Knoll, A.H., Cui, H., Wang, C., Bekker, A., Hazen, R.M., 2021. A persistently low level of atmospheric oxygen in Earth's middle age. Nat. Commun. 12, 1–7.
Liu, A., Tang, D., Shi, X., Zhou, X., Zhou, L., Shang, M., Li, Y., Fang, H., 2020. Mesoproterozoic oxygenated deep seawater recorded by early diagenetic carbonate concretions from the Member IV of the Xiamaling Formation, North China. Precambr. Res. 341, 105667.
Lu, Z., Jenkyns, H.C., Rickaby, R.E., 2010. Iodine to calcium ratios in marine carbonate as a paleo-redox proxy during oceanic anoxic events. Geology 38, 1107–1110.
Lu, Z., Hoogakker, B.A.A., Hillenbrand, C.D., Zhou, X., Thomas, E., Gutchess, K.M., Lu, W., Jones, L., Rickaby, R.E.M., 2016. Oxygen depletion recorded in upper waters of the glacial Southern Ocean. Nat. Commun. 7, 11146.
Lu, W., Ridgwell, A., Thomas, E., Hardisty, D.S., Luo, G., Algeo, T.J., Saltzman, M.R., Gill, B.C., Shen, Y., Ling, H., Edwards, C.T., Whalen, M.T., Zhou, X., Gutchess, K.M., Jin, L., Rickaby, R.E.M., Jenkyns, H.C., Lyons, T.W., Lenton, T.M., Kump, L.R., Lu, Z., 2018. Late inception of a resiliently oxygenated upper ocean. Science 361, 174–177.
Luther III, G.W., Campbell, T., 1991. Iodine speciation in the water column of the Black Sea. Deep Sea Res. Part A Oceanogr. Res. Papers 38, S875–S882.
Lyons, T.W., Reinhard, C.T., Planavsky, N.J., 2014. The rise of oxygen in Earth's early ocean and atmosphere. Nature 506, 307–315.
McIntyre, T., Fralick, P., 2017. Sedimentology and geochemistry of the 2930 Ma Red Lake-Wallace Lake Carbonate Platform, Western Superior Province, Canada. Depositional Record 3, 258–287.
Mills, D.B., Ward, L.M., Jones, C., Sweeten, B., Forth, M., Treusch, A. H., Canfield, D.E., 2014. Oxygen requirements of the earliest animals. Proc. Natl. Acad. Sci. 111, 4168–4172.
Olson, S.L., Kump, L.R., Kasting, J.F., 2013. Quantifying the areal extent and dissolved oxygen concentrations of Archean oxygen oases. Chem. Geol. 362, 35–43.
Ossa, F, Hofmann, A., Spangenberg, J.E., Poulton, S.W., Stüeken, E.E., Schoenberg, R., Eickmann, B., Wille, M., Butler, M. and Bekker, A., 2019. Limited oxygen production in the Mesoarchean ocean. Proc. Natl. Acad. Sci. 116, 6647–6652.
Ostrander, C.M., Kendall, B., Olson, S.L., Lyons, T.W., Gordon, G.W., Romaniello, S.J., Zheng, W., Reinhard, C.T., Roy, M., Anbar, A.D., 2020. An expanded shale δ^{98}Mo record permits recurrent shallow marine oxygenation during the Neoarchean. Chem. Geol. 532, 119391.
Ostrander, C.M., Johnson, A.C., Anbar, A.D., 2021. Earth's first redox revolution. Annu. Rev. Earth Planet. Sci. 49, 337–366.
Planavsky, N.J., Reinhard, C.T., Wang, X., Thomson, D., McGoldrick, P., Rainbird, R.H., Johnson, T., Fischer, W.W., Lyons, T.W., 2014. Low Mid-Proterozoic atmospheric oxygen levels and the delayed rise of animals. Science 346, 635–638.
Poulton, S.W., Canfield, D.E., 2005. Development of a sequential extraction procedure for iron: implications for iron partitioning in continentally derived particulates. Chem. Geol. 214, 209–221.
Poulton, S.W., Bekker, A., Cumming, V.M., Zerkle, A.L., Canfield, D.E., Johnston, D.T., 2021. A 200-million-year delay in permanent atmospheric oxygenation. Nature 592, 232–236.
Ramsay, B., 2017. Sedimentology and geochemistry of the 2310 Ma Kona Dolomite, Huronian Supergroup, Superior Province. Lakehead University, Thunder Bay, Canada, p. 135 pp.. BSc Thesis.
Ramsay, B., 2020. Environmental control of seawater geochemistry in a Mesoarchean peritidal system, Woman Lake, Superior Province. Lakehead University, Thunder Bay, Canada, p. 166 pp.. MSc Thesis.
Ramsay, B., Fralick, P., Bielski, P., Lalonde, S., 2020. Facies control on geochemistry of the Mesoarchean carbonate platform at Woman Lake (Canada). Goldschmidt.
Ramsay, B., Fralick, P., 2017. Sedimentology and geochemistry of the 2310 Ma Kona Dolomite, Huronian Supergroup, northwestern Ontario and western Upper Peninsula Michigan. Instit. Lake Superior Geol. 63 (Part 1), 73–74.
Rasmussen, B., Bekker, A., Fletcher, I.R., 2013. Correlation of Paleoproterozoic glaciations based on U-Pb zircon ages for tuff beds in the Transvaal and Huronian Supergroups. Earth Planet. Sci. Lett. 382, 173–180.
Reinhard, C.T., Planavsky, N.J., Robbins, L.J., Partin, C.A., Gill, B.C., Lalonde, S.V., Bekker, A., Konhauser, K.O., Lyons, T.W., 2013. Proterozoic Ocean redox and biogeochemical stasis. Proc. Natl. Acad. Sci. 110, 5357–5362.
Reinhard, C.T., Planavsky, N.J., Olson, S.L., Lyons, T.W., Erwin, D.H., 2016. Earth's oxygen cycle and the evolution of animal life. Proc. Natl. Acad. Sci. 113, 8933–8938.
Riding, R., Fralick, P., Liang, L., 2014. Identification of an Archean marine oxygen oasis. Precambr. Res. 251, 232–237.
Riding, R., Liang, L., Fralick, P., 2022. Oxygen-induced chemocline precipitation between Archean Fe-rich and Fe-poor carbonate seas. Precambr. Res. 383, 106902.
Robertson, J.A., 1973. A review of recently acquired geological data, Blind River – Elliot Lake area. Geol. Assoc. Can. Spec. Pap. 12, 169–198.
Rogers, N., 2002. Whole-rock chemical analyses from the Birch-Uchi greenstone belt, Superior Province. Geological Survey of Canada, Open File Report 4271.
Rolison, J.M., Stirling, C.H., Middag, R., Rijkenberg, M.J., 2017. Uranium stable isotope fractionation in the Black Sea: modern calibration of the $^{238}U/^{235}U$ paleo-redox proxy. Geochim. Cosmochim. Acta 203, 69–88.
Rue, E.L., Smith, G.J., Cutter, G.A., Bruland, K.W., 1997. The response of trace element redox couples to suboxic conditions in the water column. Deep Sea Res. Part I: Oceanogr. Res. Papers 44, 113–134.

Sanborn-Barrie, M., Skulski, T., Parker, J., 2001. Three hundred million years of tectonic history recorded by the Red Lake greenstone belt, Ontario. In: Current Research Part C, Geological Survey of Canada, C-19, pp. 1–19.
Schopf, J.W., 2006. Fossil evidence for Archean life. Philos. Trans. R. Soc. B 361, 869–885.
Shang, M., Tang, D., Shi, X., Zhou, L., Zhou, X., Song, H., Jiang, G., 2019. A pulse of oxygen increase in the early Mesoproterozoic Ocean at ca. 1.57–1.56 Ga. Earth Planet. Sci. Lett. 527, 115797.
Sumner, D.Y., 1997. Carbonate precipitation and oxygen stratification in late Archean seawater as deduced from facies and stratigraphy of the Gamohaan and Frisco formations, Transvaal supergroup, South Africa. Am. J. Sci. 297, 455–487.
Taylor, G.L., 1972. Stratigraphy, sedimentation and sulfide mineralization in the Kona Dolomite. Unpublished MSc. thesis, Michigan Technological University, Houghton, Michigan, U.S.A.
Thoby, M., Konhauser, K.O., Fralick, P.W., Altermann, W., Visscher, P.T., Lalonde, S.V., 2019. Global importance of oxic molybdenum sinks prior to 2.6 Ga revealed by the Mo isotope composition of Precambrian carbonates. Geology 47, 559–562.
Thurston, P.C., 1980. Subaerial volcanism in the Archean Uchi-Confederation volcanic belt. Precambr. Res. 12, 79–98.
Tostevin, R., Mills, B.J., 2020. Reconciling proxy records and models of Earth's oxygenation during the Neoproterozoic and Palaeozoic. Interface Focus 10, 20190137.
Wang, X., Ossa, F., Hofmann, A., Agangi, A., Paprika, D., Planavsky, N.J., 2020. Uranium isotope evidence for Mesoarchean biological oxygen production in shallow marine and continental settings. Earth Planet. Sci. Lett. 551, 116583.
Wohlabaugh, N., 1980. Petrology of the Big Cusp Algal Dolomite; An informal member of the Kona Dolomite, Marquette, Michigan. M.Sc. Thesis. Bowling Green State University, 164 pp.
Wood, J., 1973. Stratigraphy and sedimentation in Upper Huronian rocks of the Rawhide Lake – Flack Lake area. Geol. Assoc. Can. Spec. Pap. 12, 73–95.
Wörndle, S., Crockford, P.W., Kunzmann, M., Bui, T.H., Halverson, G.P., 2019. Linking the Bitter Springs carbon isotope anomaly and early Neoproterozoic oxygenation through I/[Ca+Mg] ratios. Chem. Geol. 524, 119–135.
Wright, D.L., Rust, B.R., 1985. Preliminary report on the stratigraphy and sedimentology of the Bar River Formation. Ontario Geol. Survey, Miscellaneous Paper 127, 119–123.
Zhang, K., Shields, G.A., 2022. Sedimentary Ce anomalies: secular change and implications for paleoenvironmental evolution. Earth Sci. Rev. 229, 104015.